Total photoabsorption cross section for ^{4}He from 200 to 800 MeV

M. MacCormick,[1,*] J. Habermann,[1,5] J. Ahrens,[4] G. Audit,[1] R. Beck,[4] A. Braghieri,[2] G. Galler,[7] N. d'Hose,[1] V. Isbert[4] P. Pedroni,[2,†] T. Pinelli,[2,3] G. Tamas,[1] S. Wartenberg,[4] and A. Zabrodin[1,6]

[1]*CEA-DAPNIA/SPhN, C.E. Saclay, F-91191 Gif sur Yvette, France*

[2]*Istituto Nazionale di Fisica Nucleare, Sezione di Pavia, via Bassi 6, I-27100 Pavia, Italy*

[3]*Dipartimento di Fisica Nucleare e Teorica, Università degli Studi di Pavia, via Bassi 6, I-27100 Pavia, Italy*

[4]*Institut für Kernphysik, Universität Mainz, I-55099 Mainz, Germany*

[5]*Physikalisches Institut, Universität Tübingen, D-72076 Tübingen, Germany*

[6]*Institute for Nuclear Research, 7a, Prospect 60 Let Oktyabrya, 117312, Moscow*

[7]*II. Physikalisches Institut, Universität Göttingen, D-37073 Göttingen, Germany*

(Received 30 August 1996)

The total photoabsorption cross section for ^{4}He has been measured for the first time over a wide photon energy range (200 MeV$\leqslant E_\gamma \leqslant$800 MeV). By using the large acceptance detector DAPHNE at the tagged photon facility of the MAMI microtron in Mainz high precision results with small systematic errors were obtained. This measurement shows that ^{4}He has a behavior similar to heavy nuclei and, in particular, a reduction of the cross section with respect to the lighter nuclei is found for $E_\gamma > 600$ MeV. [S0556-2813(97)05702-6]

PACS number(s): 25.20.−x, 13.60.Rj, 24.30.Gd

I. INTRODUCTION

The total photoabsorption cross sections ($\sigma_{\rm tot}$) for ^{1}H, ^{2}H, and ^{3}He, measured with a 4π detector, were published in a recent paper [1]. This study was instigated in order to observe the behavior of $\sigma_{\rm tot}/A$ as a function of the mass number A, and more specifically, to take a closer look at the so-called ''damping'' of the resonances that occurs beyond the Δ region (see, for example, Ref. [2]). To complete this set of data, we present in this paper the total cross section for ^{4}He.

The experimental approach has already been extensively described in [1] and [3] and will only be briefly recalled in the present paper. Specific problems concerning the extrapolation of the ^{4}He photodisintegration channels will be discussed in detail. Finally, the results for these four light nuclei will be compared with the published results for medium and heavy nuclei.

II. EXPERIMENTAL SETUP

The present experiment was performed with the 3.7 π acceptance detector DAPHNE [4], built by the DAPNIA-SPhN of Saclay and the INFN-sezione di of Pavia, that was used in conjunction with the Glasgow tagged photon facility [5] installed at the continuous wave accelerator MAMI [6] in Mainz.

The tagged photon beam was produced by bremsstrahlung of the 855 MeV electrons from MAMI on a thin gold convertor of 10^{-4} radiation lengths. The tagging system covers a photon energy range of 50–800 MeV in 352 channels each having an energy resolution of $\simeq$ 2 MeV. The collimation of the photon beam gives an experimental tagging efficiency of about 55%. A tagged photon flux of 5×10^5 s in the 200–800 MeV energy range was used during this experiment.

The photon flux was continuously measured with the aid of detectors placed in the beam downstream of the hadronic detector. Incident photons are converted into e^+e^- pairs by a 0.5 mm copper convertor and detected in coincidence by two plastic scintillator layers placed directly behind. The photon detection efficiency of this device was regularly measured, at low beam intensity, by comparison with a 100% efficient lead-glass detector. The absolute number of tagged photons is determined with a precision of $\pm 2\%$ [7].

A detailed description of DAPHNE is given in Ref. [4]. This device has a central tracking detector, consisting of three coaxial cylindrical multiwire proportional chambers, surrounded by a segmented cylindrical scintillator ΔE-E telescope for charged particle identification [8]. Finally there is a scintillator-absorber sandwich that is designed to enhance the π^0 detection efficiency and the particle identification. The main characteristics of the detector are the following: a large angular acceptance (polar acceptance: $22°\leqslant\theta\leqslant158°$ and azimuthal acceptance $0°\leqslant\phi\leqslant360°$); high precision angular measurements for charged particle trajectories [$\Delta\theta$ (FWHM) $\leqslant1°$, $\Delta\phi$ (FWHM) $\simeq2°$]; a large momentum acceptance (for protons: $p_p \geqslant$ 300 MeV/c; for pions: $p_\pi \geqslant$ 78 MeV/c); good proton/pion particle discrimination as long as the proton has $p_p \leqslant$ 900 MeV/c; good proton momentum resolution ($\Delta p_p/p_p$=2.5–10 % in the measured range); a modest but useful π^0 efficiency ($\simeq$20% for the 2 photons of the π^0 decay required in coincidence).

The liquid ^{4}He target at 4.25 K and 1050 mbar is contained in a Mylar cylinder of dimensions 4.3 cm in diameter by 27.5 cm in length. Liquefaction was obtained with a Gifford-MacMahon ^{4}He refrigerator coupled to a Joule-

*Present address: GANIL, Bd. Henri Bequerel, F-14000, CAEN, France.

†Author to whom correspondence should be addressed at INFN–Sezione di Pavia, via Bassi 6, I-27100 Pavia, Italy. Electronic address: PEDRONI@PAVIA.INFN.IT

Thomson expansion valve which provides the pressure reduction necessary in order to reach the low temperature. The cryogenic system was automatically regulated and all critical parameters relating to the target environment were continuously recorded [9]. Under the operating conditions the stability of the target density was of the order of 0.5%.

III. DATA ANALYSIS

We briefly recall the general principles of the data analysis method that is fully described in [1]. From 65% (at 300 MeV) to 80% (at 700 MeV) of the total cross section is directly accessed by measuring the number of events with charged particles in the final state. About 80% of the remaining part is deduced from the measured number of π^0 events with no accompanying charged particle by using the calculated π^0 detection efficiency. Finally, the last contribution is evaluated by the extrapolation of the charged pion photoproduction channels and of the photodisintegration channels over the polar angular and momentum regions that are outside the DAPHNE acceptance.

Using the same notation introduced in [1], the total cross section can be written as

$$\sigma_{\rm tot}=C[N_{\rm ch}+N_{\pi^0}(\overline{\epsilon_{\pi^0}})^{-1}+\Delta N_{\pi^\pm}+\Delta N_p], \qquad (1)$$

where

$$C=\frac{1}{N_\gamma N_T}$$

and $N_{\rm ch}$ is the total number of charged events detected; N_{π^0} is the total number of unaccompanied π^0's detected; $\overline{\epsilon_{\pi^0}}$ is the calculated π^0 detection efficiency; $\Delta N_{\pi^\pm}$ is the sum of all the corrections and extrapolations for charged pions; ΔN_p is the sum of all the corrections and extrapolations for the photodisintegration channels; N_γ is the total number of photons; and N_T is the total number of target atoms.

In [1] we discussed in detail the extrapolation method applied to the photodisintegration channels in the case of ^{2}H and ^{3}He. For ^{4}He, the extrapolation procedure is not so straightforward since the cross sections of main photodisintegration processes are not known. These channels are as follows: the the two nucleon ($2N$) process, that is the photoabsorption by a pn pair with the remaining two nucleons as spectators: $\gamma+{}^4{\rm He}\rightarrow pn+n_s+p_s$; the two processes that account for the photoabsorption by three nucleons ($3N$): $\gamma+{}^4{\rm He}\rightarrow ppn+n_s$ and $\gamma+{}^4{\rm He}\rightarrow pnn+p_s$ (these two processes should have similar cross sections); the four nucleon ($4N$) absorption process which, according to the results of pion absorption experiments (Refs. [10–12]) must also be taken into account.

Both the $\gamma+{}^4{\rm He}\rightarrow p+t$ and $\gamma+{}^4{\rm He}\rightarrow p+d+n_s$ channels have a very small cross section for $E_\gamma>200$ MeV and they were not given any special consideration in the extrapolation procedure.

Since in all photodisintegration processes at least one energetic proton is emitted, the extrapolation procedure was performed starting with the single proton spectra. The first step in the analysis was to separate between the photodisintegration and the pion photoproduction channels. For all single proton events the photon energy (E_γ), the proton momentum (p_p) and the proton laboratory angle (θ_p) are known, and so the invariant mass (M_X) of the undetected system can be constructed, with

$$M_X^2=(E_\gamma+M_{^4{\rm He}}-E_p)^2-(\vec{p}_\gamma-\vec{p}_p)^2.$$

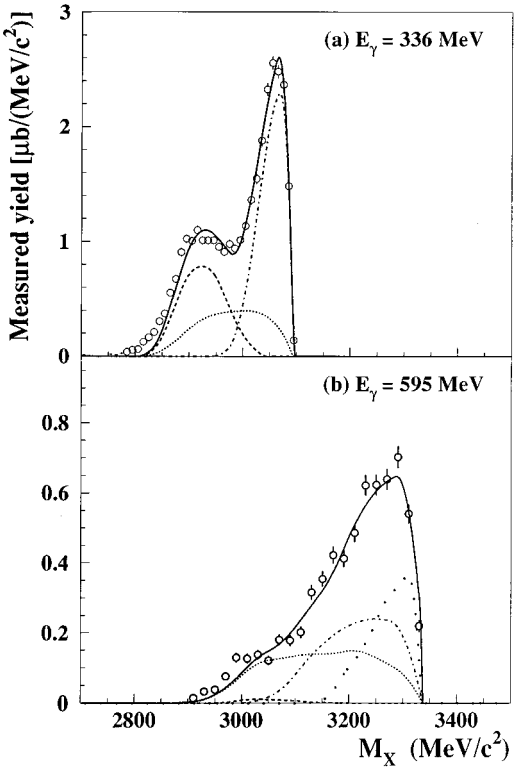

FIG. 1. M_X distribution at $E_\gamma=340$ MeV (a) and $E_\gamma=590$ MeV (b). Open circles represent the experimental data while the different style lines indicate the different contribution as calculated by the fitting procedure. Dashed line: $2N$ photoabsorption; short-dotted line: $(3N+4N)$ photoabsorption; dash-dotted line: single pion photoproduction processes; long-dotted line: contribution of double pion photoproduction processes; continuous line: sum of all previous contributions.

Figure 1 shows the invariant mass spectra at $E_\gamma=336$ MeV (a) and $E_\gamma=595$ MeV (b). Below 260 MeV, as the protons emitted in photoproduction processes are too low in kinetic energy to reach the detector, there is only one peak, corresponding to photodisintegration processes. At 336 MeV [Fig. 1(a)] the peak at $M_X\simeq3050$ MeV, corresponding to protons from the single pion photoproduction channels, can be clearly seen. At higher energy [Fig. 1(b)] the peak at $M_X\simeq3300$ MeV is larger as double pion production processes occur and make up the dominant contribution.

The different partial channels are then separated with the aid of a Monte Carlo simulation which takes into account the following.

(i) The detector acceptances and resolutions in θ, ϕ, and p_p.

(ii) The angular distributions of the pion photoproduction channels. The $\gamma+p\rightarrow p+\pi^0$ channel was simulated using the data from Ref. [13] while a uniform phase space distribution was assumed for the $\gamma+p\rightarrow p+\pi+\pi$ channels.

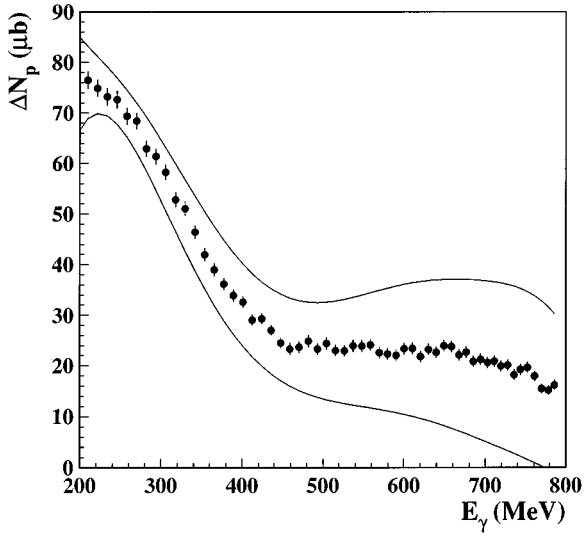

FIG. 2. Calculated missing contribution ΔN_p of the photodisintegration channels (solid dots). The two continuous lines represent the extreme values obtained with all the different hypotheses made in the fitting procedure.

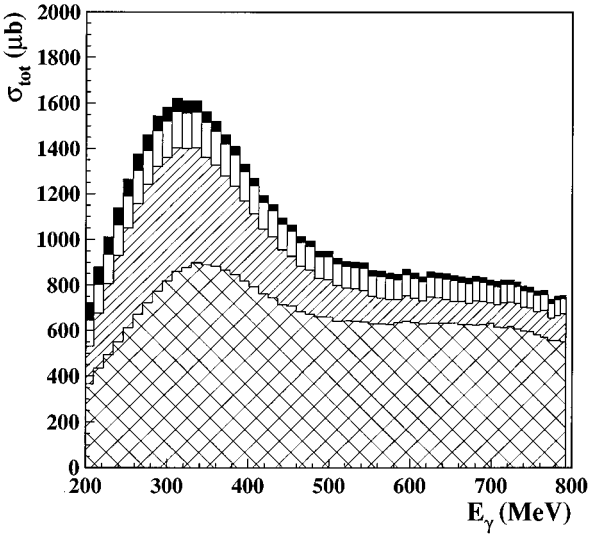

FIG. 4. The individual contributions to the total photoabsorption cross section for ^{4}He [see Eq. (1)] are shown by the different hatched areas. N_{ch}: double hatched area; $N_{\pi 0}(\overline{\epsilon_{\pi 0}})^{-1}$: diagonal hatched area; $\Delta N_{\pi^\pm}$: vertical hatched area; ΔN_p: black area.

(iii) The angular distributions of the photodisintegration channels. For the $2N$ (pn) process the angular distribution was taken from [7] and a uniform phase space distribution for both $3N$ $(ppn$ and $pnn)$ and $4N$ $(ppnn)$ contributions was assumed.

(iv) The Fermi motion of the interacting proton. For the quasifree photoproduction processes, the Fermi momentum distribution of the interacting nucleon was taken from the ^{4}He$(e,e'p)$ experiment of Ref. [14]. This distribution, however, does not take into account final state interactions (FSI's) whose effects cannot be completely ignored. The effect of FSI has been clearly shown both in the $\gamma+D\rightarrow p+p+\pi^-$ channel (Ref. [15]) and in the π absorption experiments (Refs. [10–12]). To take this into account, the overall fitting procedure was repeated adding a flat tail from 180 MeV/c up to 300 MeV/c (the DAPHNE proton

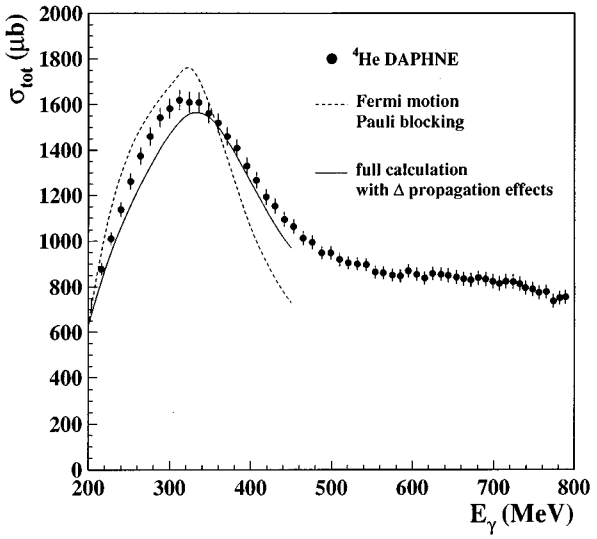

FIG. 3. The total photoabsorption cross section for ^{4}He measured in the present experiment (solid dots) is compared with the model of Ref. [16]. Dashed line: calculation taking into account only Fermi motion and Pauli blocking; continuous line: full model with the inclusion of Δ propagation effects. The experimental error bars represent the linear sum of the statistical and the systematic errors.

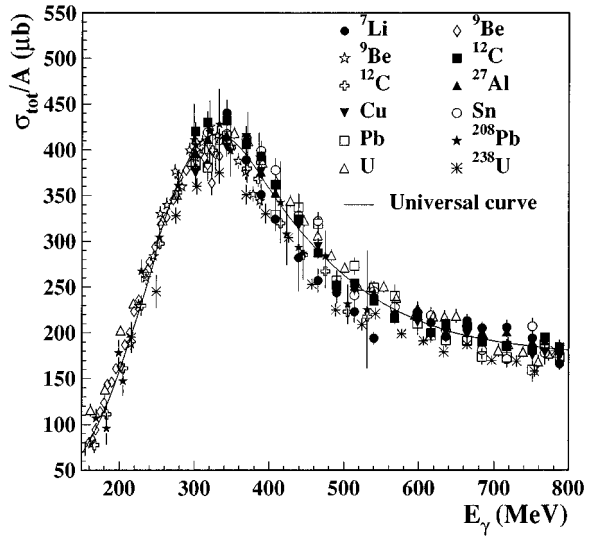

FIG. 5. Experimental total photoabsorption cross sections per nucleon values in the photon energy range 200–800 MeV for a variety of medium and heavy nuclei: ^{7}Li [2] (solid circles), ^{9}Be [18] (open diamonds), ^{9}Be [19] (open stars), ^{12}C [2] (solid squares), ^{12}C [20] (open crosses), ^{27}Al [2] (solid triangles), Cu [2] (solid inverse triangles), Sn [2] (open dots), Pb [2] (open squares), ^{208}Pb [20] (solid stars), U (averaged on ^{235}U and ^{238}U) [21] (open triangles), and ^{238}U [22] (asterisks). Only statistical errors are shown. For sake of clarity, only a part of the total data has been shown. The continuous line represents the average of all published results.

TABLE I. The total photoabsorption cross sections (in μb) for ^{4}He determined for 57 photon energy bins centered on the specified value of E_γ. Both statistical ($\pm\Delta\sigma_{\rm stat}$) and systematic errors ($\pm\Delta\sigma_{\rm syst}$) are given.

E_γ (MeV)	$\sigma_{\rm tot}$ (μb)	$\Delta\sigma_{\rm stat}$ (μb)	$\Delta\sigma_{\rm syst}$ (μb)	E_γ (MeV)	$\sigma_{\rm tot}$ (μb)	$\Delta\sigma_{\rm stat}$ (μb)	$\Delta\sigma_{\rm syst}$ (μb)	E_γ (MeV)	$\sigma_{\rm tot}$ (μb)	$\Delta\sigma_{\rm stat}$ (μb)	$\Delta\sigma_{\rm syst}$ (μb)
204	722	2	23	430	1154	4	30	635	855	5	26
216	879	3	25	442	1095	4	28	644	851	5	26
228	1010	3	27	453	1064	4	28	654	842	5	26
240	1139	3	30	465	1013	4	27	663	836	5	26
252	1263	3	32	476	995	4	26	672	831	5	26
264	1374	4	35	488	950	4	25	681	839	5	26
276	1461	4	37	499	949	4	25	690	834	5	26
288	1543	4	39	510	920	4	25	699	823	5	26
300	1583	4	40	521	905	4	25	707	814	5	26
312	1620	4	41	532	901	4	25	715	824	5	27
324	1610	4	41	543	897	5	25	723	823	5	27
336	1610	4	41	554	865	4	24	731	814	5	27
348	1563	4	39	564	862	5	25	739	795	5	26
360	1521	4	38	575	852	5	24	747	789	5	26
371	1462	4	37	585	847	5	25	756	775	5	26
383	1410	4	36	595	870	5	25	765	778	5	26
395	1332	4	34	605	855	5	25	774	737	5	25
407	1269	4	32	615	839	5	25	782	751	5	25
419	1194	4	31	625	859	5	26	789	756	6	25

threshold) to the momentum distribution of Ref. [14]. A comparison of the results stemming from these two different hypotheses on the Fermi momentum distribution allows an estimation of the associated systematic error.

The results of the fitting procedure are shown in Fig. 1 by the different style lines. The measured photodisintegration cross section was then obtained by subtracting the final photoproduction contribution from the experimental spectra. This contribution was then used to evaluate the extrapolations that need to be done before the final total photodisintegration cross section could be determined. As the aim here is not to separate $2N$, $3N$, and $4N$ cross sections, but to obtain an estimation of the systematic errors in the extrapolation of all photodisintegration processes, two further hypotheses were made. The fitting procedure was performed with the supposition that the total photodisintegration cross section is due only either to $2N$ absorption [$\gamma+{}^4\mathrm{He}\rightarrow p+n+(np)_s$], or to $3N$ and $4N$ photodisintegration processes. The cross sections for the three reactions, $\gamma+{}^4\mathrm{He}\rightarrow ppn+n_s$, $\gamma+{}^4\mathrm{He}\rightarrow pnn+p_s$, $\gamma+{}^4\mathrm{He}\rightarrow ppnn$, were taken as being equal.

The final results are shown in Fig. 2. The two continuous lines correspond to the extreme values obtained by all the fitting procedures that were performed under the different hypotheses made. In the final determination of the total photoabsorption cross section we have taken the average value of the different results obtained for the extrapolation. The associated systematic uncertainty was taken as being half the difference between the extreme values. The extrapolations are seen to be small compared to the total cross section values and the corresponding systematic error reaches a maximum of ± 16 μb at 700 MeV, which corresponds to less than 2% of the total cross section.

IV. RESULTS AND COMMENTS

The total photoabsorption cross section for ^{4}He is depicted in Fig. 3, and the corresponding values are listed in Table I. Figure 4 shows the individual contributions according to Eq. (1).

The dashed line in Fig. 3 corresponds to a calculation [16] which takes into account only the Fermi momentum, the nucleon binding energy, and Pauli corrections accounting for the blocking of the Δ decay into the occupied nucleon states and coherent photoproduction. This calculation, done in the framework of a shell model, does not satisfactorily reproduce the experimental data. A better agreement is clearly obtained when medium corrections for the Δ propagation are included, as shown by the continuous line in Fig. 3. In this approach the essential mechanism is due to the nuclear excitation of Δ-hole components and their subsequent propagation through the nuclear medium. The parameters of the potential describing this propagation were derived from pion-nucleus scattering, so that no free parameters were introduced in the photoabsorption calculation. Considering the fact that in this calculation the Born terms are added in an approximate way, the agreement with the data can be considered as satisfactory. The Δ-hole model which takes into account the Δ nuclear decay channels gives a good description of the quenching of the cross section around the resonance peak and of the broadening of the distribution. A similar kind of calculation, done for ^{12}C and ^{208}Pb [17] gives the same good agreement with the data.

Previous data for a variety of nuclei, ranging from ^{7}Li to ^{238}U, show that $\sigma_{\rm tot}/A$ is constant to within the experimental uncertainties and it is therefore possible to use a ''universal curve'' as an average behavior of all published results for medium and heavy nuclei (see Fig. 5).

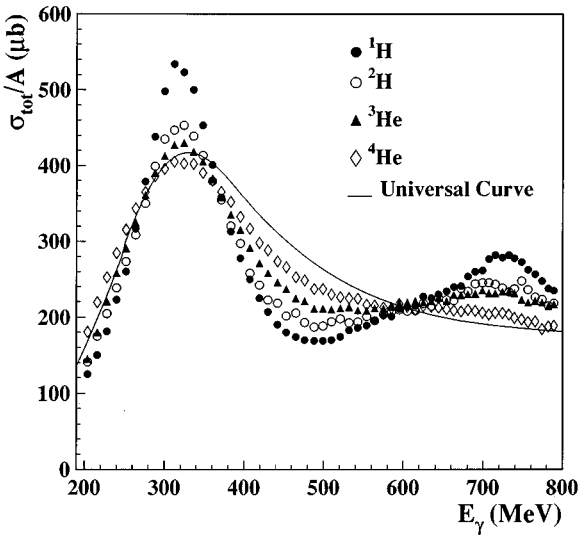

FIG. 6. The total photoabsorption cross sections per nucleon from 200 MeV to 800 MeV for ^{1}H (solid circles), ^{2}H (open circles), ^{3}He (solid triangles), and ^{4}He (open diamonds) are compared to the ''universal curve'' for medium and heavy nuclei. Statistical errors are included but are smaller than the symbols' size.

In Fig. 6 the present data on ^{4}He are compared with the complementary set of ^{1}H, ^{2}H, and ^{3}He results from [1] and with the ''universal curve'' of Fig. 5.

The large increase of σ_{tot}/A versus A (see Fig. 6) in the region 350–450 MeV may be due, as suggested by Carrasco and Oset [23], to the production on a single nucleon of off-shell pions which can subsequently be reabsorbed by other nucleons since, in this region, the phase space accessible for double pion photoproduction is enlargened with respect to the free-nucleon case. To test this hypothesis, it would be interesting to measure all individual partial channels and to compare the photoproduction and the photodisintegration cross sections since their ratio is expected to vary as a function of A.

In the second resonance region, above 450 MeV, the ^{4}He cross section follows the same behavior as the heavier nuclei, giving rise to a smoothly decreasing curve which has no prominent features. The mechanisms responsible for this apparent ''damping'' of the resonances is not well understood and several approaches have been proposed [24–26]. It is worth pointing out that, according to two recent calculations [27,28], the main contribution to the double pion photoproduction on the proton is, in this energy range, the direct production of a $\Delta\pi$ state. The contribution of the D_{13} resonance is small and appears essentially through its interference with this main mechanism. Consequently, one can expect that the same kind of Δ-hole calculation will also explain, in this region, an important part of the quenching of the cross section. Besides this theoretical work, a measurement of the cross sections for all individual partial channels is needed to give a better insight into this problem.

V. CONCLUSION

The total photoabsorption cross section measurement for ^{4}He over the photon energy range 200–800 MeV has completed the study carried out on light nuclei in order to explore the evolution of nuclear medium effects in the transition from hydrogen to heavy nuclei. This complete set of data shows clearly the nuclear resonances' deformation in going from ^{1}H to ^{4}He and will provide a strong constraint to the microscopic theoretical treatments that are needed to explain the so-called ''damping'' of the higher resonances.

[1] M. MacCormick *et al.*, Phys. Rev. C **53**, 41 (1996).
[2] N. Bianchi *et al.*, LNF Report No. 95/053 (1995); Phys. Rev. C **54**, 1688 (1996).
[3] M. MacCormick, Ph.D. thesis No. 2981, Université de Paris Sud, Orsay, 1993; C.E. Saclay Report No. DAPNIA/SPhN 93 63 (1993).
[4] G. Audit *et al.*, Nucl. Instrum. Methods Phys. Res. A **301**, 473 (1991).
[5] S. Hall, G. J. Miller, R. Beck, and P. Jennewein, Nucl. Instrum. Methods Phys. Res. A **368**, 698 (1996).
[6] H. Herminghaus, A. Feder, K. H. Kaiser, W. Manz, and H v.d. Schmitt, Nucl. Instrum. Methods Phys. Res. A **138**, 1 (1976).
[7] R. Crawford *et al.*, Nucl. Phys. **A603**, 303 (1996).
[8] A. Braghieri *et al.*, Nucl. Instrum. Methods Phys. Res. A **343**, 623 (1994).
[9] B. Hervieux *et al.*, Comptes Rendus des Quatrièmes Journées d'Aussois, Aussois 1993 (CNRS Grenoble).
[10] M. Steinacher *et al.*, Nucl. Phys. **A517**, 413 (1990).
[11] P. Weber *et al.*, Phys. Rev. C **43**, 1553 (1991).
[12] E. Daum *et al.*, Nucl. Phys. **A589**, 553 (1995).
[13] H. Genzel, P. Joos, and W. Pfeil, in *Photoproduction of Elementary Particles*, edited by H. Schopper, Landolt-Börnstein, New Series, Group 1, Vol. 8 (Springer-Verlag, Berlin, 1973).
[14] V. A. Goldstein *et al.*, Nucl. Phys. **A355**, 333 (1981).
[15] P. Benz *et al.*, Nucl. Phys. **B65**, 158 (1973).
[16] J. H. Koch, E. J. Monitz, and N. Ohtsuka, Ann. Phys. (N.Y.) **154**, 99 (1984).
[17] R. C. Carrasco and E. Oset, Nucl. Phys. **A536**, 445 (1992); **A541**, 585 (1992).
[18] J. Ahrens, H. Gimm, R. J. Hughes, R. Leicht, P. Minn, A. Ziegler, and B. Ziegler, in *Photopion Nuclear Physics*, edited by P. Stoler (Plenum Press, New York, 1979), p. 275.
[19] J. Arends, J. Eyink, A. Hegerath, K. G. Hilger, B. Mecking, G. Nodelke, and H. Rost, Phys. Lett. **98B**, 423 (1981).
[20] R. Bergère, in *Proceedings II Workshop on Perspectives in Nuclear Physics at Intermediate energies*, Trieste, 1985, edited by S. Boffi, C. Ciofi degli Atti, and M. M. Giannini (World Scientific, Singapore, 1985), p. 153; L. Ghedira, Ph.D. thesis No. 2967, Université de Paris Sud, Orsay, 1984.
[21] Th. Frommhold, F. Steiper, W. Henkel, and U. Kneissl, Phys. Lett. B **295**, 28 (1992); Th. Frommhold *et al.*, Z. Phys. A **350**, 249 (1994).
[22] N. Bianchi *et al.*, Phys. Lett. B **299**, 219 (1993).
[23] J. A. Gomez Tejedor, M. J. Vicente-Vacas, and E. Oset, Nucl. Phys. **A588**, 819 (1995).
[24] M. M. Giannini and E. Santopinto, Phys. Rev. C **49**, R1258 (1994).

[25] W. M. Alberico, G. Gervino, and A. Lavagno, Phys. Lett. B **321**, 177 (1994).

[26] S. V. Akulinichev and A. I. L'vov, Mainz Internal Report No. MKPH-T-93-1, 1993.

[27] J. A. Gomez Tejedor and E. Oset, Nucl. Phys. **A600**, 413 (1996).

[28] J. M. Laget and L. Y. Murphy, C. E. Saclay Report No. DAPNIA/SPhN-96-10 (1996); submitted to Nucl. Phys. A.